ACS ES&T Water

pubs.acs.org/estwater

Article

Phosphate Recovery by a Surface-Immobilized Cerium Affinity Peptide

Zihang Su, Jacob D. Hostert, and Julie N. Renner*

Cite This: *ACS EST Water* 2021, 1, 58–67

Read Online

ACCESS | Metrics & More | Article Recommendations | Supporting Information

ABSTRACT: Cerium oxide/hydroxide adsorbents have emerged as promising phosphate removal materials due to their excellent performance and stability. In this study, an engineered cerium affinity peptide immobilized on a metal surface was utilized to synthesize a novel, nanoscale, and bio-enabled phosphate adsorbent. The goal of this work was to characterize the binding of phosphate and potential competing ions to the novel material, demonstrating the potential utility of the engineered peptide in biotemplating applications. Phosphate binding and competing ion binding with time were investigated via a quartz crystal microbalance with dissipation (QCM-D). Kinetic modeling of the QCM-D data revealed that the bio-enabled material facilitated strong phosphate adsorption behavior in a wide pH range of 3−7. Changing the media from simple phosphate solutions to more complex synthetic wastewater solutions did not negatively impact the observed binding constants. The main phosphate adsorption mechanism likely followed a ligand exchange process, with enhanced adsorption achieved by increasing the number of surficial hydroxide groups. The strong binding behavior observed with phosphate was not observed when the material was exposed to common competing ions. Overall, this study presents a sequence-defined peptide as a promising tool for the engineering of advanced phosphate capture materials.

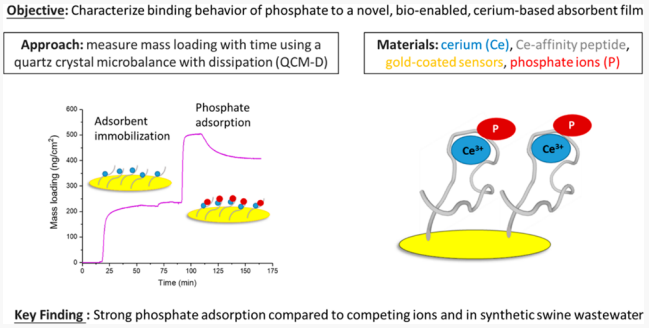

KEYWORDS: *phosphorus, adsorption, surface immobilization, peptides, cerium*

Phosphorus is an essential nutrient for all living organisms, generally in the form of phosphate ions; its availability and accessibility are important to human society.[1] However, as a nonrenewable resource, and with growing demand over the past few decades, it has been estimated that phosphate supplies will be depleted in the second half of this century.[2] In addition, due to industrial and agricultural activities, excess phosphorus readily accumulates in natural water bodies, which causes eutrophication that threatens aquatic ecosystems.[3,4] Motivated by dwindling phosphate resources and the need to control phosphate levels in water systems, removal and recycling of excess phosphate from water bodies has become an urgent societal issue.

A variety of strategies have been implemented to treat phosphorus-rich water bodies efficiently. Chemical precipitation is a reliable and well-established process, using iron, aluminum, magnesium, and calcium salts to react with soluble phosphate to form solid precipitates.[5,6] However, precipitation is limited by pH and is inefficient at low phosphate concentrations. Enhanced biological phosphorus removal requires a low level of chemical usage and can remove the vast majority of phosphate; however, the range of ideal applicable conditions is narrow, and they need to be strictly controlled.[7] In addition, physical methods such as membrane processes (e.g., electrodialysis, reverse osmosis, and nanofiltration) provide excellent phosphate removal but often have low selectivity and incur high costs.[8,9] Compared to the treatments described above, processes based on adsorption represent promising and feasible ways to recover phosphate. Metal oxide/hydroxide-based adsorption has been one of the most successful methods and has the following advantages: low cost, effective at low phosphate concentrations, operable in a wide working pH range, and simple to operate. Various metal-based adsorbents have been reported for phosphate capture, such as Al, Ca, Fe, Mg, Zn, and rare-earth metals.[10,11]

One of the most abundant rare-earth metals, cerium, has shown a high affinity for phosphate and stability over a range of pH conditions. However, few studies have been reported on Ce-based phosphate removal processes, with a lack of development of Ce-based materials in contrast to other metals.[12−14] The inclusion of cerium in materials has been shown to increase the phosphate adsorption capacity. For

Received: June 2, 2020
Revised: June 30, 2020
Accepted: July 20, 2020
Published: August 11, 2020

https://dx.doi.org/10.1021/acsestwater.0c00001
ACS EST Water 2021, 1, 58–67

example, Gu et al. fabricated zinc ferrite doped with cerium and achieved an improved phosphate adsorption capacity that increased from 5.2 to 41.6 mg/g at 25 °C, showing good selectivity in the presence of competing anions.[15] Su et al. synthesized mesoporous Ce−Zr binary oxide nanoparticles and reported an excellent adsorption capacity of 112.23 mg/g.[14]

Increasing the surface area of the metal oxide/hydroxide adsorbent by utilizing a support material is often desired. The selection of a support material depends on many factors, including cost, adherence of the metal oxide/hydroxide to the support, and mechanical integrity and stability under the desired conditions, which can vary.[11] The use of bio-derived supports for cerium-based phosphate adsorbents is becoming a promising, cost-effective approach to materials design. For instance, fibrous proteins,[16] chitosan,[17] and aminated lignin[18] have been utilized as supports for cerium-based phosphate recovery. However, like non-bio-derived options, it is difficult to tailor the structural and chemical properties of the composite materials, which represents a major challenge.[11] One way to overcome this challenge is through the use of engineered peptides/polypeptides, which have recently emerged as powerful templates for the synthesis of highly controlled, environmentally friendly, inorganic materials.[19] However, to date there have been no reports of engineered peptides being used to develop materials for phosphate capture, which is the subject of this study.

EF-hand peptide sequences containing helix−loop−helix motifs have strong affinities for Ce(III) ions[20,21] and thus are promising candidates for cerium-based adsorbent design. We have shown in a previous study that immobilized EF-hand peptides have the same affinity for Ce(III) ions as the same free peptide in solution.[22] To demonstrate the potential for engineered peptides/polypeptides to be used in the development of advanced phosphate capture materials, we designed an EF-hand peptide to specifically capture cerium while immobilized on a gold substrate and characterized the ability of the peptide−cerium film to adsorb phosphate in complex environments.

To assess the binding of phosphate to the peptide−cerium films, a quartz crystal microbalance with dissipation (QCM-D), a highly sensitive technique used to analyze molecular adsorption, was applied in this study. Briefly, QCM-D sensors resonate at a known frequency, and as material adsorbs to the sensor, the relative frequency shifts, signifying a change in hydrated mass. The QCM-D enables the determination of the amount of adsorbed material on a surface at the nanogram level and the viscoelastic properties of adsorbed layers in real time,[23,24] which also allows kinetic modeling to be conducted on the data. The QCM-D sensors can be subsequently subjected to surface analysis techniques such as Fourier-transform infrared spectroscopy (FTIR), X-ray photoelectron spectroscopy (XPS), or time-of-flight secondary ion mass spectrometry (TOF-SIMS) to confirm the chemical nature of the adsorbed material.

The objective of this study was to characterize the binding of phosphate, and potential competing ions, to an immobilized cerium-loaded peptide to demonstrate its potential utility in biotemplating and/or development of bio-enabled materials. The cerium-loaded engineered peptide was expected to facilitate binding of phosphate to the solid substrate. Phosphate adsorption was examined via the QCM-D under different pH and ionic strength conditions, and in simple phosphate solutions as well as synthetic wastewater. A kinetic adsorption model was derived and applied to understand the binding mechanism. The components captured on the gold surface were characterized using advanced surface characterization techniques. Overall, the results demonstrated the ability of the engineered peptide to be applied in metal-based material synthesis for efficient phosphate capture for the first time.

MATERIALS AND METHODS

Materials. Deionized water used in all experiments was obtained from Western Reserve Water Systems mixed deionizer tanks (10 MΩ). Nitrogen gas (N_2, 99.99%) was obtained from Airgas for drying. Sodium dodecyl sulfate ($C_{12}H_{25}NaO_4S$, 99%) was purchased from Hoefer for QCM-D module cleaning. For quartz crystal sensor cleaning, a hydrogen peroxide solution (H_2O_2, 25%) was purchased from Sigma-Aldrich and an ammonium hydroxide solution (NH_4OH, 30%) was purchased from Alfa Aesar. Other chemicals, including cerium chloride heptahydrate (99.9%), were purchased from Sigma-Aldrich. Calcium chloride dehydrate (99.0−105.0%), hydrochloric acid (0.995−1.005 N) solution, anhydrous sodium sulfate (≥99.0%), sodium hydroxide pellets (≥97.0%), and sodium phosphate monobasic monohydrate (99.9%) were purchased from Fisher Scientific. Ammonium phosphate monobasic (98%) and magnesium chloride hexahydrate (99−102%) were obtained from VWR. Ammonium chloride (ACS grade) and HEPES sodium salt were obtained from Dot Scientific. Potassium chloride (99%) was purchased from Alfa Aesar.

Peptide Design. The peptide sequence chosen for this study (Figure S1) was derived from loop I of calmodulin[25] and previously shown by our group to bind to cerium(III) ions when immobilized to gold.[22] Briefly, the calmodulin-derived sequence was modified to bind to gold by incorporating a cysteine on the N-terminus. A flexible glycine spacer was used to avoid conformationally constraining the calmodulin-derived sequence. The N- and C-termini were acetylated and amidated, respectively. The resultant sequence, CGGGDKDGDGTITTKE, was purchased from GenScript at ≥95% purity.

Characterization of Adsorption Behavior. *QCM-D Experiments.* A QCM-D (QSense Explorer, controlled by Q-Soft integrated software from Biolin Scientific) was used to investigate the adsorption of the peptide on gold-coated QCM sensors, as well as adsorption of cerium and phosphate on the peptide and cerium-loaded peptide, respectively. Desorption of phosphate was also monitored by a solvent rinse. All experiments were conducted in aqueous solutions. The frequency shifts and dissipation changes were monitored simultaneously over time. Frequency shifts reflect the mass gain and loss on the crystal sensor surface, while the dissipation changes provide the information about the viscoelastic and mechanical properties of adsorbed layers.[26] Cleaning procedures and equations used for QCM-D data analysis can be found in our previous work.[27] Briefly, all experiments were performed in a flow module at a rate of 150 μL min^{-1} and at 18 °C with clean gold-coated quartz crystal sensors (QSX 301, 5 MHz, Biolin Scientific). All experiments consisted of establishing a stable baseline (defined as a <0.5 Hz frequency shift over 10 min) before a new solution was added. Baseline solvent solutions were used to rinse the unbound molecules before the introduction of new solutions. All QCM-D data were analyzed by QSense Dfind Software (Biolin Scientific), and the fifth overtone (25 MHz) was used in all data analysis. All experiments were performed in at least triplicate (n = 3),

https://dx.doi.org/10.1021/acsestwater.0c00001
ACS EST Water 2021, 1, 58−67

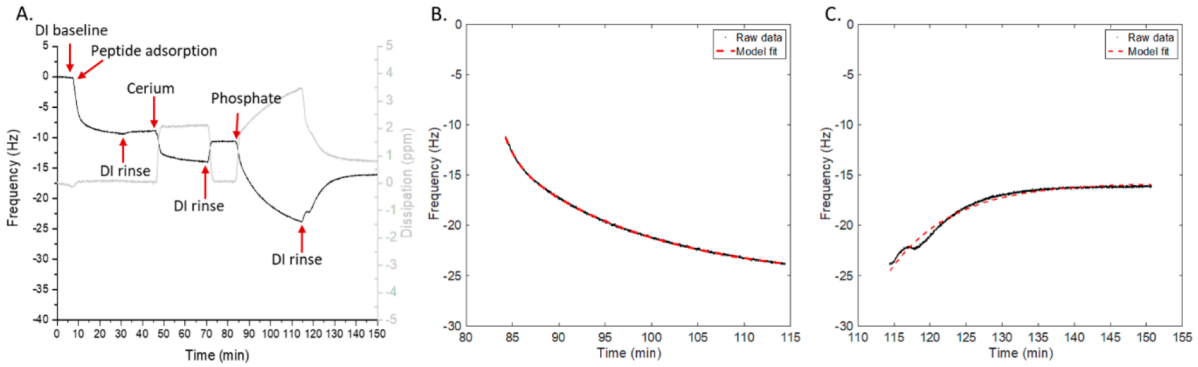

Figure 1. Kinetic characterization of adsorption and desorption of phosphate to peptide−cerium films reveals a potential binding mechanism. (A) Relative frequency (black) and dissipation (grey) shifts vs. time of a representative QCM-D experiment where first a stable peptide−cerium film was formed and then phosphate adsorption was performed, followed by desorption. Red arrows indicate when different solutions were introduced into the sensor. (B) Modeling of phosphate adsorption data on the cerium−peptide immobilized film. (C) Modeling of phosphate desorption data during the final DI water rinse process. Red dashed lines represent results of nonlinear least-squares curve fitting in panels B and C, performed using MATLAB.

unless otherwise noted. The dissipation change was always low throughout the experiments (<5% of the frequency change), indicating rigid layers were formed; therefore, a composite Sauerbrey model was used for data analysis.[28,29]

Synthesis of the Peptide−Cerium Layer and Characterization of Phosphate Adsorption. Deionized (DI) water served as the baseline solution prior to the experiment, and then 10 μg mL^{-1} peptide in DI water was introduced into the QCM-D flow module to functionalize the gold-coated crystal surface. Relative frequency shifts and dissipation changes were monitored with time simultaneously. After peptide adsorption, DI water was utilized to rinse weakly bound molecules and stabilize the frequency for ∼10 min. Then, a 1 mM $CeCl_3$ solution was pumped into the flow module until the frequency stabilized, and DI water was pumped for 10 min to rinse.

After a stable peptide−cerium layer was achieved, a 1 mM Na_2HPO_4 (pH 9.2) solution was introduced, and phosphate binding was monitored for approximately 30 min using the QCM-D. After phosphate binding, DI water (pH ∼6.5) was introduced to monitor desorption behavior until the frequency stabilized. Similar experiments were performed using neutral (pH 7.2) HEPES buffer ($C_8H_{18}N_2O_4S$) as the baseline for phosphate adsorption and desorption experiments. Note that HEPES served as a baseline for peptide and cerium adsorption as well in these neutral buffer experiments only. Kinetic models were applied to the adsorption and desorption data to understand binding behavior as explained in Notes 1−5 of the Supporting Information.

We chose to investigate the potential of this technology to remove phosphate from swine wastewater, as it has been suggested that alternative treatments for the recovery of phosphorus from swine manure are needed to prevent losses of phosphorus to the environment.[30] Various synthetic swine wastewater compositions have been reported in studies of phosphate removal.[31−33] The synthetic wastewater (pH 5) was made by adding 438 mg of $MgSO_4{\cdot}7H_2O$, 961 mg of NH_4Cl, 104 mg of $NH_4H_2PO_4$ and 132 mg of $CaCl_2{\cdot}H_2O$ to 450 mL of DI water. Synthetic swine wastewater solutions were introduced into the QCM module after the assembly of cerium on the peptide in DI water. To test the binding at neutral pH, the pH was adjusted to 7 by using a 0.1 M NaOH solution. The kinetic binding behavior at pH 7 was modeled and compared to the model of binding of phosphate to peptide−cerium films in pH 7.2 HEPES buffer.

Figure S2 summarizes each step of the process for forming the peptide−cerium film on a gold-coated QCM-D sensor and analyzing the adsorption of ions to the film, including (1) peptide assembly followed by a solvent rinse, (2) cerium binding followed by a solvent rinse, and (3) ion capture followed by a solvent rinse.

Influence of pH on Phosphate Adsorption. The influence of pH on the adsorption of phosphate to the cerium−phosphate films was investigated with the QCM-D. The pH of the 1 mM Na_2HPO_4 solution was adjusted to 3 or 12 using 0.1 M HCl or NaOH, respectively. After exposure to the phosphate solutions with the adjusted pH, DI water was used as the final rinse.

Influence of Exposure to Competing Ions. Using the QCM-D, competitive ions were tested to preliminarily screen the selectivity of the peptide for cerium ions, and the selectivity of peptide−cerium films for phosphate. The competing ions were prepared at concentrations higher than those of the target cerium or phosphate ions. Binding of the peptide to Ca^{2+} ions (using 10 mM to 1 M $CaCl_2$ in DI water) was characterized, and the behavior was compared to that of cerium. The binding of a representative common competing ion SO_4^{2-} (using 250 mM Na_2SO_4 in DI water) to the peptide−cerium film was characterized, and the behavior was compared to that of phosphate ions.

Influence of Ionic Strength on Phosphate Adsorption. Additional QCM-D experiments were performed in the presence of a 100 mM KCl solution where the adsorbed peptide was exposed to 100 mM KCl as the new baseline. The peptide was then exposed to solutions of $CeCl_3$ (1 mM) and then Na_2HPO_4 (1 mM) in 100 mM KCl. This served as a general test of phosphate binding in the presence of higher-ionic strength solutions (vs DI water).[34] The KCl solution was used to rinse between steps until the very end of the experiment when DI water was introduced as a final rinse.

Surface Characterization of Peptide−Cerium Adsorbent Films. *Fourier-Transform Infrared Spectroscopy (FTIR).* The presence of the peptide, cerium, and phosphate on the gold-coated QCM-D sensor was confirmed by using Fourier-transform infrared spectroscopy (FTIR). A Nicolet iS50R FT-IR (ThermoFisher Scientific) spectrometer, equipped with a

https://dx.doi.org/10.1021/acsestwater.0c00001
ACS EST Water 2021, 1, 58−67

mercury cadmium telluride (MCT) detector and a VeeMAX III accessory adjusted to 80°, was used. Before all experiments, the system was purged with pure nitrogen gas and cooled with liquid nitrogen for 30 min. All samples were made via the QCM-D process. A clean bare gold sensor spectrum was collected first and subtracted from sample spectra taken with appropriate baseline corrections. All spectra were collected with 2000 scans and a scan resolution of 8000 cm^{-1}.

X-ray Photoelectron Spectroscopy (XPS). X-ray photoelectron spectroscopy (XPS) experiments were performed with a PHI Versa Probe 5000 instrument on gold-coated QCM-D sensor samples to confirm the presence of cerium on peptide-functionalized samples. A monochromatic Al Kα X-ray source ($h\nu$ = 1486.6 eV) was utilized. Survey scans were performed with a 100 μm beam diameter and an analyzer pass energy of 117.40 eV. The samples were prepared from QCM-D experiments.

Time-of-Flight Secondary Ion Mass Spectrometry (TOF-SIMS). TOF-SIMS (time-of-flight secondary ion mass spectrometry) was used to confirm the presence of thiols (cysteine from peptides) and phosphate on the surface of the gold-coated QCM-D sensors. The acquisition was made in negative mode, and the 30 kV Ga gun was operated in bunched mode (aperture size of 100 μm). The raster size was 100 μm × 100 μm. All samples were prepared from QCM-D experiments.

RESULTS AND DISCUSSION

Characterization of Adsorption and Desorption of Phosphate to Peptide−Cerium Films. The QCM-D was used to study the adsorption and desorption of phosphate to the assembled cerium−peptide films. In QCM-D experiments, negative or positive frequency shifts reflect a mass increase or loss on the gold surface, and dissipation shifts correspond to the mechanical properties of the assembled layer. Figure 1A depicts the relative frequency shifts and dissipation changes of a representative QCM-D experiment, where red arrows indicate when different solutions were introduced into the flow module. Repeat experiments can be found in Figure S3. To prepare the peptide−cerium films, DI water served as a baseline, and then peptides were immobilized to the surface (the first negative frequency shift), followed by a rinse with DI water. Then cerium binding occurred (the second negative frequency shift) when the $CeCl_3$ solution was introduced, followed by a rinse with DI water till the frequency stabilized. The adsorption of cerium to the immobilized peptides was analyzed in our previous study,[22] where we found the dissociation constant (K_D) to be 1.3 ± 0.1 μM.

Once a stable peptide−cerium film was formed, a 1 mM Na_2HPO_4 solution in DI water was added to the system for ∼30 min to study phosphate adsorption, and then DI water was introduced to rinse the loosely accumulated ions and study phosphate desorption. To ensure all binding observed was hydrated phosphate, no other ions were added to the system; thus, the pH was not adjusted. DI water had a pH of ∼6.5, and the 1 mM solution of Na_2HPO_4 had a pH of 9.2. The frequency decreased while the dissipation increased upon addition of phosphate ions, suggesting the salt ions accumulated on the surface. Upon the introduction of DI water, a positive frequency shift occurred with a negative shift in dissipation, indicating the desorption of weakly accumulated ions. The final frequency stabilized at a value that was lower than the initial level of the stable peptide−cerium film, showing that strongly bound material from the phosphate solution remained on the surface. We estimated the amount of hydrated phosphate that was strongly bound under these specific conditions and time frames to be 0.29 ± 0.08 g of hydrated phosphate/g of hydrated peptide−cerium film [average ± standard error (n = 6)]. While a direct comparison of this value to those of other materials is not appropriate due to the varying conditions, the varying techniques, and in this case the hydrated nature of the measurement, we note that the adsorption capacity of cerium-functionalized materials, specifically cerium−zirconium binary oxide nanoparticles, has been reported to be as high as 0.112 g/g.[14]

To further investigate the adsorption behavior, a kinetic model was utilized to fit the data. The derivation of the kinetic model can be found in Note 1 of the Supporting Information. The reaction scheme chosen for the model is shown below:

$$A + B \underset{k_d}{\overset{k_a}{\rightleftharpoons}} AB^*$$

$$A + B \xrightarrow{k_t} AB$$

where A represents phosphate ions and B represents the sites available for binding. AB and AB* represent the strongly adsorbed and weakly adsorbed species, respectively. In this model, it is assumed that the formation of the strongly adsorbed complex is relatively irreversible. The model derived from the reaction scheme presented above is biexponential, represented by eq 1:

$$F = B_0[1 - e^{-(k_t A)t}] + \frac{k_a A B_0^*}{k_a A + k_d}[1 - e^{-(k_a A + k_d)t}] \quad (1)$$

where F is the relative frequency in hertz, B_0* is the maximum possible frequency shift due to weak phosphate binding (units of hertz, proportional to mass), B_0 represents the maximum possible frequency shift due to strong binding (units of hertz, proportional to mass), A is the concentration of phosphate ions (molar), t is the time (seconds), k_a represents the forward reaction rate constant (M^{-1} s^{-1}), k_d represents the reverse reaction rate constant (s^{-1}), and k_t represents the rate constant associated with strong binding (M^{-1} s^{-1}). Prior to fitting, the x axis was normalized by subtracting the time when the adsorption started and the y axis was normalized by subtracting the initial frequency. Nonlinear curve fitting was performed using MATLAB® to obtain B_0, k_tA, B_0*, k_aA, and k_d.

Figure 1B shows a representative adsorption data set fit to the model described in eq 1. A first-order fit and a second-order fit were also attempted, but they did not describe the data as well as the biexponential (see Table S1), suggesting that the model selected for adsorption is appropriate.

For desorption, the equations in Note 1 of the Supporting Information were adjusted for the special case in which the phosphate concentration was zero (see the derivation in Note 2 of the Supporting Information). The model reduced to a single-exponential form represented by eq 2:

$$F = F_0 + F_0^* e^{-k_d t} \quad (2)$$

where F is the frequency, F_0 (hertz) corresponds to the initial frequency shift due to strongly adsorbed phosphate, and F_0* represents the initial frequency shift due to weakly adsorbed phosphate. The rate of desorption is represented by k_d (s^{-1}). Nonlinear curve fitting was performed after normalizing the y axis by subtracting the initial frequency prior to adsorption and normalizing the x axis by subtracting the time desorption

https://dx.doi.org/10.1021/acsestwater.0c00001
ACS EST Water 2021, 1, 58−67

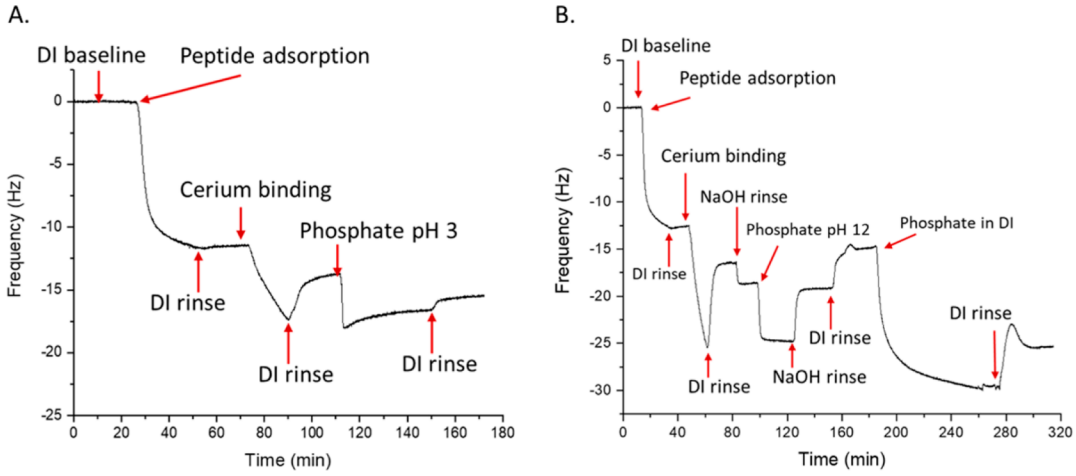

Figure 2. QCM-D experiments demonstrate that pH has a significant impact on the adsorption of phosphate to peptide−cerium films. Peptide and cerium adsorption occurred in DI water prior to exposure at extreme pH values. (A) Peptide−cerium films exposed to 1 mM Na_2HPO_4 (pH 3). (B) Peptide−cerium films exposed to 1 mM Na_2HPO_4 (pH 12), followed by re-exposure of the film to 1 mM Na_2HPO_4 in DI water (pH 9.2). Red arrows indicate when different solutions were introduced into the sensor.

started to obtain F_0, F_0*, and k_d. Figure 1C shows representative desorption data fit to the model described in eq 2. A second-order fit was also attempted, but it did not describe the data as well as eq 2 (see Table S1), suggesting that the model selected for desorption was appropriate.

Control experiments were performed to analyze the binding of phosphate to the peptide with no cerium (Figure S4A). Without cerium, the peptide-functionalized surface exhibited weak affinity for phosphate ions, where any frequency decrease on the sensor was completely reversed upon exposure to DI water. This behavior was distinctly different from that observed when cerium was present. Phosphate also had similar behavior when interacting with bare gold (Figure S4B). The adsorption and desorption of phosphate to both the peptide only and bare gold could be modeled by the equations derived in Note 3 of the Supporting Information, where there was no irreversible binding step. This model fits better than a second-order model and is equivalent to a first-order model (see Table S2).

Overall, the kinetic analysis of adsorption and desorption of phosphate to peptide−cerium films indicated that the process occurred in two concurrent steps characterized by weak reversible ion accumulation and relatively strong binding. Strong binding occurs only in the presence of cerium, indicating that cerium bound to the peptide is capable of phosphate capture.

Once the models were selected, QCM-D monitoring of the adsorption of phosphate on peptide−cerium films was conducted in neutral (pH 7.2) HEPES buffer to investigate the adsorption kinetics in a more relevant water environment seen in wastewater. In Figure S5, HEPES buffer served as the baseline, carrier, and rinsing solution. A significant negative frequency shift represented the binding of phosphate on the surface, and a minor positive frequency shift reflected the desorption upon rinsing with HEPES buffer. The models described in Notes 1 and 2 of the Supporting Information were applied to the adsorption and desorption curves at pH 7.2; k_aA, k_d, and k_tA were estimated from adsorption to be ∼4.7, 2.8×10^{-3}, and 8.1×10^{-2} s^{-1}, respectively (reported in Table S3). We found that the same models that could be applied in simple solutions could also be applied in pH 7.2 HEPES buffer, indicating the same binding mechanism was employed.

Influence of pH on Phosphate Adsorption. The effect of solution pH on the adsorption of phosphate by the peptide−cerium film was investigated with QCM-D. Figure 2 shows frequency shifts with time when the films were exposed to phosphate under acidic (Figure 2A) and basic (Figure 2B) conditions. In Figure 2A, a solution of 1 mM Na_2HPO_4 adjusted to pH 3 was introduced after the peptide−cerium film had been stabilized, and DI water was used for a final rinse. Upon exposure to acidic Na_2HPO_4, a negative frequency shift was observed, indicating phosphate adsorbed to the surface. After the final DI water rinse, the frequency decrease compared to the previous DI water rinse was lower and thus related only to strongly bound phosphate captured on the surface. Therefore, at pH 3, behavior similar to that observed in Figure 1 was observed. In Figure 2B, a pH 12 NaOH solution was used to rinse after the formation of a stable peptide−cerium film and a solution of 1 mM Na_2HPO_4 adjusted to pH 12 was introduced after the rinse. A clear frequency decrease can be observed after NaOH was introduced, which we speculate is hydroxyl ions captured by cerium on the surface. Then the 1 mM Na_2HPO_4 solution at pH 12 was introduced, and a negative frequency shift occurred but was completely reversed after a further NaOH rinse, indicating weak ion accumulation was occurring without a strong binding step. To investigate the reversibility of the high-pH effect, a DI water rinse was performed and a 1 mM Na_2HPO_4 solution (same as Figure 1A, pH 9.2) was pumped in. A significant negative frequency shift was observed, with the frequency remaining low upon rinsing, indicating the recovery of the behavior observed in Figure 1 where strong binding also took place. Notably, the amount of strongly bound phosphate that was present after exposure to NaOH was more than in the experiments in Figure 1 (∼5 Hz greater frequency shift observed). This phenomenon could be due to more Ce−OH formation during the high-pH treatment. The additional −OH groups may have remained on the cerium after a DI water rinse, thus providing more active binding sites for phosphate adsorption.[35,36] pH is a critical parameter that affects phosphate adsorption. It has been well accepted that the dominant mechanism of adsorption of phosphate to a metal-based adsorbent is inner-sphere complexation via ligand

https://dx.doi.org/10.1021/acsestwater.0c00001
ACS EST Water 2021, 1, 58−67

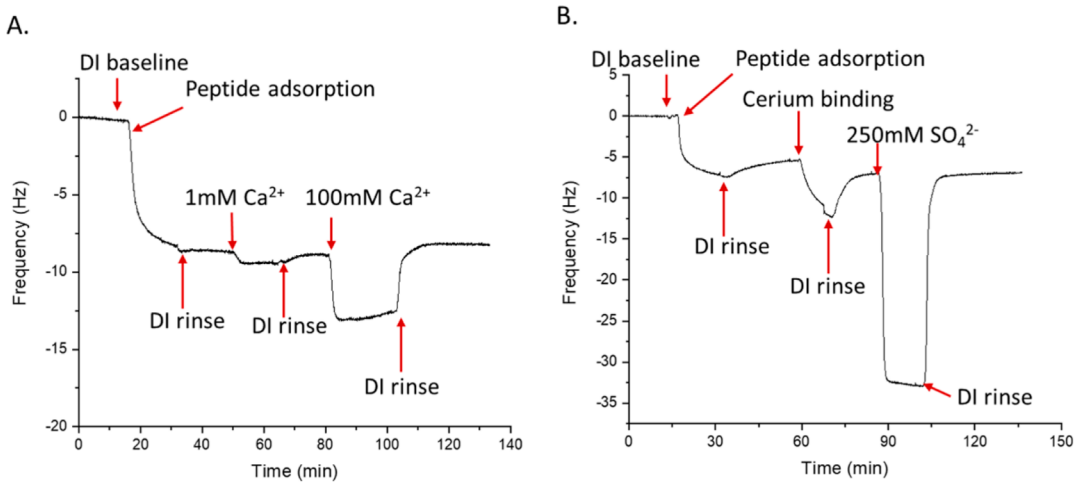

Figure 3. QCM-D monitoring of frequency changes vs. time reveals weaker binding of selected competitor ions to the peptide−cerium films compared to phosphate. (A) Calcium, a potential competing cation for adsorption of cerium on the peptide, was assessed by introducing solutions of $CaCl_2$ (1 mM) to a peptide-functionalized gold-coated sensor, performing a DI water rinse, introducing a higher concentration of calcium ions (100 mM), and performing a final DI water rinse. (B) Sulfate, a potential competing anion for adsorption of phosphate on the peptide−cerium film, was assessed by introducing a 250 mM Na_2SO_4 solution after stable peptide−cerium film formation followed by a DI water rinse. Red arrows indicate when a new solution was introduced into the QCM-D sensor.

exchange between phosphate and hydroxyl groups.[37] However, other processes of electrostatic force and hydrogen bonds have also been reported. Under aqueous conditions, phosphate species can exist as H_3PO_4, $H_2PO_4^-$, HPO_4^{2-}, and PO_4^{3-} (pK_a values of 2.1, 7.2, and 12.3).[10] When the pH increases, deprotonation processes occur on metal-based adsorbents, leading to more negative surficial charge. In addition, as the pH increases, there are more negatively charged phosphate species, and electrostatic force changes from attraction to repulsion between adsorbents and phosphate.[38] Moreover, the ligand exchange process releases hydroxyl groups and prefers acidic conditions. At high pH, competition between phosphate ions and the excessive hydroxyl groups has been cited to decrease phosphate adsorption.[39]

The results show that strong binding preferentially occurs under acidic conditions, while at pH 12, due to the electrostatic repulsion and hydroxyl competition, strong binding no longer occurs. This phenomenon can be reversed by changing the environmental pH conditions, demonstrating the reusability and stability of this adsorbent. Moreover, this behavior provides the potential to improve surface functional sites of the peptide−cerium adsorbent under high-pH condition treatments, showing the ability to further enhance phosphate adsorption. Overall, our results corroborate the findings that pH is a critical parameter affecting the adsorption mechanisms of phosphate aqueous solutions and are similar to those of previous studies, in which the maximum adsorption capacity for cerium materials is under acidic to neutral conditions.[15,16,18,40]

Influence of Competing Ions on the Assembled Peptide−Cerium Films. Selectivity is an important factor for metal-based adsorbent design when considering use in a complicated wastewater environment.[41] Selected ions were introduced to the peptide−cerium films, and adsorption behavior was monitored using the QCM-D. In this study, we chose common ions found in wastewater sources, including Ca^{2+}, a cation that could affect the adsorption of cerium to the peptide, and SO_4^{2-}, a representative anion that has been reported to influence the adsorption of phosphate to metal-based adsorbents and biotemplated hybrid films.[42,43]

Figure 3A shows QCM-D experiments performed with Ca^{2+}. In this experiment, calcium ions were added after peptide immobilization and subjected to a DI water rinse. Then, a higher-concentration calcium solution was introduced, followed by a final DI water rinse. Calcium ions appeared to have a weaker affinity for the peptide, as evidenced by the complete rinsing off of the ions upon exposure to DI water at both low and high concentrations, where the relative frequency returned to the same value that was found prior to the introduction of a calcium solution. The adsorption behavior is very similar when calcium chloride is exposed to bare gold (Figure S6A). These experiments imply that the affinity of the bound peptide for calcium ions is not as strong as that for cerium under these conditions, which has also been observed previously in solution.[25] We also note that phosphate did not demonstrate the same binding behavior when introduced into the peptide exposed to calcium instead of cerium (Figure S6B). The presence of calcium can form coprecipitates with phosphate (Ca−P);[44,45] however, the precipitates showed no affinity for the peptide layer. These results in Figure 3A and panels A and B of Figure S6 suggest that the peptide has a high affinity for cerium and that calcium is not a competing ion that will disturb phosphate adsorption.

Figure 3B shows the results of a QCM-D experiment in which the peptide−cerium film was exposed to 250 mM Na_2SO_4 in DI water, followed by a DI water rinse. In wastewater, multivalent anions with a higher charge density have been reported to nonspecifically adsorb more easily.[46] In this experiment, it was observed that at a high concentration of SO_4^{2-}, the frequency decreased but returned to the original value upon exposure to a DI water rinse. This behavior was distinctly different than when the film was exposed to phosphate (at 1 mM), where strongly bound material remained upon a DI water rinse. This different behavior suggests sulfate is not a strong competitor in the adsorption of phosphate process to our peptide−cerium film.

https://dx.doi.org/10.1021/acsestwater.0c00001
ACS EST Water 2021, 1, 58−67

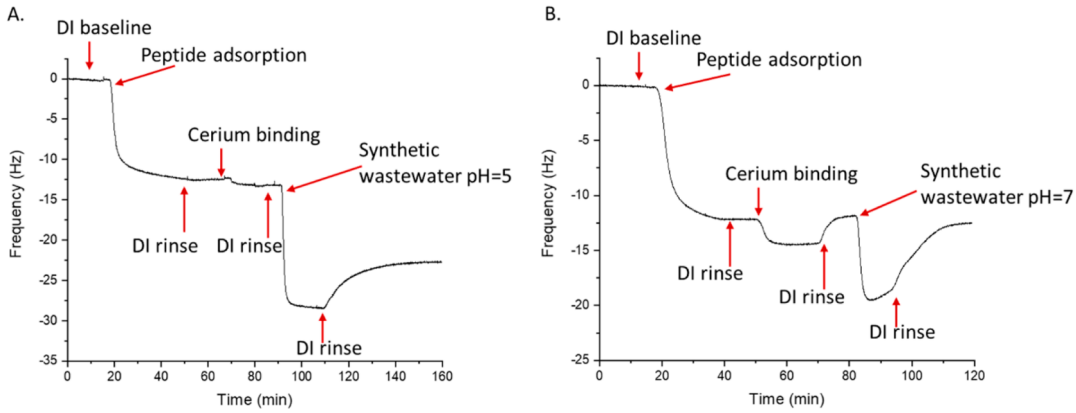

Figure 4. QCM-D monitoring of relative frequency shifts vs. time for peptide−cerium films exposed to synthetic wastewater reveals similar binding behavior compared to that in simple buffered solutions. (A) Stable peptide−cerium film exposed to synthetic wastewater at pH 5. (B) Stable peptide−cerium film exposed to synthetic wastewater at pH 7. DI water was used as the baseline and the final rinse.

Characterization of Phosphate Adsorption in Synthetic Wastewater. Prior to the synthetic wastewater testing, the effect of ionic strength on the adsorption of phosphate to the peptide−cerium film was evaluated in 100 mM KCl as the carrier and rinse solution (Figure S7).[47] Phosphate appeared to adsorb, and the smaller frequency shift after a KCl rinse indicated strongly bound phosphate remained on the peptide−cerium surface in the KCl environment. To investigate the behavior in complicated water environments, phosphate adsorption of the peptide−cerium film in a synthetic wastewater medium was tested via a QCM-D, and the samples were characterized by surface analysis methods described in the next section to confirm the presence of phosphate and other surface components. A synthetic wastewater solution containing Mg^{2+}, SO_4^{2-}, NH_4^+, Cl^-, and Ca^{2+} mixed with phosphate was introduced after the peptide−cerium film formed, followed by a DI water rinse (Figure 4). The difference in frequency between the final DI water rinse and the stabilized peptide−cerium film was attributed to strongly bound phosphate. As shown in Figure 4A, upon exposure to pH 5 wastewater, a significant permanent frequency decrease of ∼9 Hz indicated strongly bound material adsorbed to the peptide−cerium film, whereas the strongly bound material corresponded to ∼1 Hz at pH 7 (Figure 4B). The results of repeat QCM-D experiments in synthetic wastewater can be found in Figure S8. We attributed the different binding in this time frame to the effect of pH, where more acidic conditions contribute to stronger electrostatic attraction between the adsorbent and phosphate ions, decreasing the binding energy of dominant phosphate species and providing a favorable environment for ligand exchange. This observation matched our previous pH effect results and is supported by other studies, as well, which have observed a higher level of phosphate binding under acidic conditions.[13,16,18,48] Control experiments with synthetic wastewater (pH 7) exposed to bare gold-coated crystal sensors and exposed to the peptide without cerium can be found in Figure S9. Generally, no strongly bound materials remained after a DI water rinse on bare gold or on peptide films without cerium.

The QCM-D adsorption data obtained when the peptide−cerium films were exposed to synthetic wastewater at pH 7 were modeled using eq 1 to obtain kinetic constants [R^2 = 0.996 (Figure S10)]. Table S3 shows the results of the modeling, and that the constants are generally comparable (on the same order of magnitude) as constants found when modeling phosphate adsorption in HEPES buffer at pH 7 using eq 1. The constant k_t, associated with the relatively strong phosphate binding that occurs only in the presence of cerium, was found to be ∼0.07 s^{-1} mM^{-1} in the synthetic wastewater experiment at pH 7, compared to ∼0.08 s^{-1} mM^{-1} in HEPES buffer at pH 7. The agreement of the constants further supports the assumption that phosphate is adsorbing via the same mechanism in both experiments. Thus, the model may be useful for estimating the length of time to reach equilibrium at a given phosphate concentration (Figure S11).

Surface Characterization of Peptide−Cerium Adsorbent Films. The composition of the gold surface after functionalization with peptide, cerium, and phosphate was investigated by FTIR, XPS, and TOF-SIMS. All samples consisted of gold-coated crystal surfaces with components assembled via the QCM-D. Rinse steps with DI water and nitrogen drying were always employed prior to analysis. Figure 5 summarizes the FTIR spectra of samples of the peptide assembled on the gold surface, peptide−cerium films, peptide−cerium films exposed to a simple phosphate solution [1 mM Na_2PO_4 (pH 9.2)], and peptide−cerium films exposed to synthetic wastewater (pH 5). All samples were scanned in the range of 4000 to 650 cm^{-1} and are represented with the gold background subtracted. The peaks at 1650 cm^{-1} (blue dashed lines) were assigned to amide I vibrations from C═O stretching and confirmed the presence of the peptide on gold because C═O is a main component of the peptide backbone.[49] The peaks at 3400 cm^{-1} (green dashed lines) were assigned to −OH stretching vibrations from Ce−OH groups.[50] These peaks appeared in samples exposed to cerium ions (all samples except peptide only). In Figure 5D, the significant decrease in −OH vibrations compared to Figure 5B was attributed mainly to phosphate adsorption and supported a ligand exchange mechanism. The adsorption of cerium on peptide-functionalized gold surfaces was also confirmed by XPS, as shown in Figure S12.

The FTIR peaks observed around 1050 cm^{-1} (red dashed lines) were assigned to a combination of the asymmetric stretching vibrations of P−O and the stretching vibrations of P═O.[51] These strong adsorption peaks appeared when the peptide−cerium film was exposed to phosphate in solution, confirming that phosphate binds to the peptide−cerium film upon exposure to simple solutions, as well as synthetic

https://dx.doi.org/10.1021/acsestwater.0c00001
ACS EST Water 2021, 1, 58−67

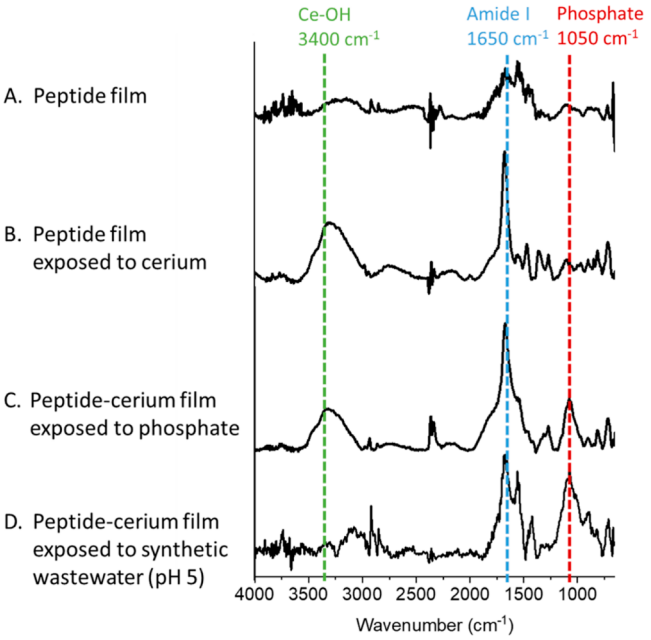

Figure 5. FTIR confirms the presence of phosphate in peptide−cerium films. Spectra of (A) the peptide assembled on a gold crystal sensor, (B) the peptide assembled layer exposed to a cerium solution ($CeCl_3$), (C) the peptide−cerium film exposed to a phosphate solution (1 mM Na_2HPO_4), and (D) the peptide−cerium film exposed to synthetic wastewater at pH 5.

wastewater at pH 5. It was observed that the intensity of the hydroxyl peak at 3400 cm^{-1} relatively decreased after the peptide−cerium film was exposed to a simple phosphate solution. A relatively larger decrease in the intensity of the hydroxyl peak was observed after exposure to synthetic wastewater at pH 5. This decrease at 3400 cm^{-1} was attributed to the formation of more Ce−O−P coordination bonds that replaced Ce−OH bonds. The synthetic wastewater experiment was conducted at a lower pH compared to the pH 9 phosphate adsorption experiment, which was thought to enhance electrostatic interactions as well as ligand exchange, as discussed in the previous section.

The presence of O−P−O groups and sulfur in samples exposed to synthetic wastewater (pH 7) was also confirmed by TOF-SIMS (Figure 6). When the data are normalized to total counts, there is an order of magnitude increase in the magnitude of the O−P−O signal and the S signal in the wastewater sample compared to those of bare gold, indicating the presence of phosphate and the attachment of peptides. Overall, the surface characterizations demonstrate that the peptide−cerium films were viable in complex environments and capable of binding phosphate.

CONCLUSIONS

In this work, an engineered peptide assembled on gold was utilized to immobilize cerium, forming a novel adsorbent film for phosphate capture. We aimed to characterize the binding of phosphate, and potential competing ions, to the peptide-facilitated adsorbent film to demonstrate the capacity of the engineered peptide to be utilized in bio-enabled materials development. The binding behavior was analyzed via a QCM-D, and kinetic modeling revealed that the presence of cerium enabled strong phosphate adsorption versus more reversible weak adsorption, which occurs on samples without cerium. Testing performed under different pH conditions suggested the strong phosphate binding behavior preferentially occurred in a wide acidic pH range (3−7) for peptide−cerium films. The level of strong binding decreased with an increase in pH and disappeared at pH 12. The adsorption mechanism likely followed inner-sphere complexation via a ligand exchange

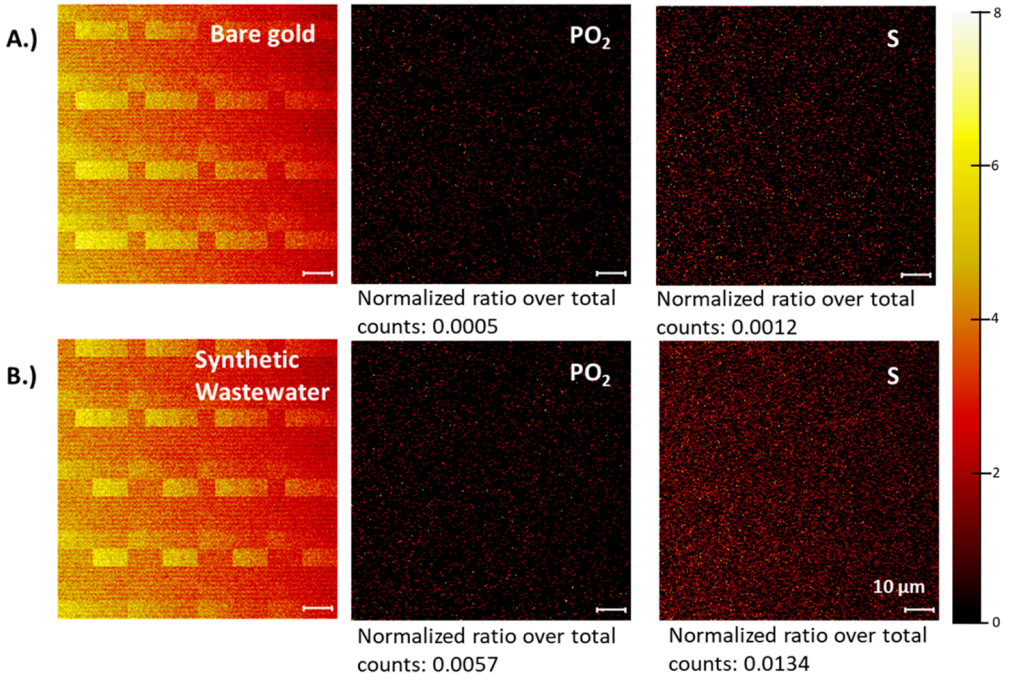

Figure 6. TOF-SIMS mapping of the total secondary ions acquired in negative mode (left) and the normalized ratio of O−P−O groups (middle) and sulfur bonds (right) over the total counts. The top sample (A) is the bare gold-coated crystal sensor, and (B) the bottom sample is the peptide−cerium functionalized gold-coated crystal sensor exposed to simulated wastewater (pH 7). Samples were made via QCM-D.

https://dx.doi.org/10.1021/acsestwater.0c00001
ACS EST Water 2021, 1, 58−67

process. The adsorption performance was improved by base pretreatment, suggesting further performance enhancement may be possible by modifying the material with surficial hydroxyl functional groups. QCM-D monitoring of selected competing ion adsorption revealed that the bound peptide has a greater affinity for cerium ions than for calcium ions. In addition, sulfate, a competitor ion for phosphate adsorption, did not exhibit the same strong binding behavior as phosphate on the peptide−cerium films. The strong binding of phosphate to peptide−cerium films was also maintained under high-ionic strength conditions. Upon exposure to synthetic wastewater, strong adsorption behavior was observed, and the kinetic binding constants were comparable to those of simple buffered solutions, suggesting similar binding mechanisms were being used. In general, this work introduces a novel way to create advanced phosphate capture materials with high phosphate affinity in relevant wastewater environments, via the use of engineered peptides. Future work will expand on the applications of this peptide to bind cerium to other substrates, and advanced material characterization techniques will be utilized to understand the impact of the peptide on cerium distribution in those materials. By utilizing the peptide to control the attachment of cerium, new materials for a range of different wastewater environments can be created.

■ ASSOCIATED CONTENT

Supporting Information

The Supporting Information is available free of charge at https://pubs.acs.org/doi/10.1021/acsestwater.0c00001.

Figures S1−S12, Tables S1−S3, and Notes 1−5 (PDF)

■ AUTHOR INFORMATION

Corresponding Author

Julie N. Renner − *Department of Chemical and Biomolecular Engineering, Case Western Reserve University, Cleveland, Ohio 44106, United States;* orcid.org/0000-0002-6140-4346; Email: jxr484@case.edu

Authors

Zihang Su − *Department of Chemical and Biomolecular Engineering, Case Western Reserve University, Cleveland, Ohio 44106, United States;* orcid.org/0000-0001-6216-6880

Jacob D. Hostert − *Department of Chemical and Biomolecular Engineering, Case Western Reserve University, Cleveland, Ohio 44106, United States;* orcid.org/0000-0003-3519-7002

Complete contact information is available at: https://pubs.acs.org/10.1021/acsestwater.0c00001

Author Contributions

This manuscript was written through contributions of all authors. All authors have given approval to the final version of the manuscript. Specifically, Z.S. conducted all of the experiments shown, performed data analysis, and was the primary author responsible for writing the manuscript. J.D.H. conducted all kinetic modeling and analysis and contributed to the editing of the manuscript. J.N.R. designed experiments, analyzed data, and worked closely with the student team to write the manuscript.

Notes

The authors declare no competing financial interest.

■ ACKNOWLEDGMENTS

This work was supported by the U.S. Department of Agriculture (Award 2018-68011-28691) and the National Science Foundation (Award 1739473). The authors thank Craig Bishop and Dr. Tae Kyong John Kim from the Swagelok Center for Surface Analysis of Materials (SCSAM) located at Case Western Reserve University for helping obtain TOF-SIMS and XPS data. The authors also appreciate Dr. Lauren Greenlee of University of Arkansas (Fayetteville, AR) for the helpful discussion of our results.

■ REFERENCES

(1) Karl, D. M. Phosphorus, the staff of life. *Nature* **2000**, *406*, 31−33.

(2) Van Vuuren, D. P.; Bouwman, A. F.; Beusen, A. H. W. Phosphorus demand for the 1970-2100 period: A scenario analysis of resource depletion. *Glob. Environ. Chang.* **2010**, *20*, 428−439.

(3) Dodds, W. K.; et al. Eutrophication of U. S. freshwaters: Analysis of potential economic damages. *Environ. Sci. Technol.* **2009**, *43*, 12−19.

(4) Mayer, B. K.; et al. Total Value of Phosphorus Recovery. *Environ. Sci. Technol.* **2016**, *50*, 6606−6620.

(5) Xie, F.; et al. Removal of phosphate from eutrophic lakes through adsorption by in situ formation of magnesium hydroxide from diatomite. *Environ. Sci. Technol.* **2014**, *48*, 582−590.

(6) Xu, Y.; et al. PH dependent phosphorus release from waste activated sludge: Contributions of phosphorus speciation. *Chem. Eng. J.* **2015**, *267*, 260−265.

(7) Gebremariam, S. Y.; Beutel, M. W.; Christian, D.; Hess, T. F. Research Advances and Challenges in the Microbiology of Enhanced Biological Phosphorus Removal-A Critical Review. *Water Environ. Res.* **2011**, *83*, 195−219.

(8) Bacelo, H.; Pintor, A. M. A.; Santos, S. C. R.; Boaventura, R. A. R.; Botelho, C. M. S. Performance and prospects of different adsorbents for phosphorus uptake and recovery from water. *Chem. Eng. J.* **2020**, *381*, 122566.

(9) De-Bashan, L. E.; Bashan, Y. Recent advances in removing phosphorus from wastewater and its future use as fertilizer (1997-2003). *Water Res.* **2004**, *38*, 4222−4246.

(10) Wu, B.; Wan, J.; Zhang, Y.; Pan, B.; Lo, I. M. C. Selective Phosphate Removal from Water and Wastewater using Sorption: Process Fundamentals and Removal Mechanisms. *Environ. Sci. Technol.* **2020**, *54*, 50−66, DOI: 10.1021/acs.est.9b05569.

(11) Liu, R.; et al. Review of metal (hydr)oxide and other adsorptive materials for phosphate removal from water. *J. Environ. Chem. Eng.* **2018**, *6*, 5269−5286.

(12) Wang, L.; et al. Development of rare earth element doped magnetic biochars with enhanced phosphate adsorption performance. *Colloids Surf., A* **2019**, *561*, 236−243.

(13) Guo, H.; et al. A study of phosphate adsorption by different temperature treated hydrous cerium oxides. *Rare Met.* **2011**, *30*, 58−62.

(14) Su, Y.; Yang, W.; Sun, W.; Li, Q.; Shang, J. K. Synthesis of mesoporous cerium-zirconium binary oxide nanoadsorbents by a solvothermal process and their effective adsorption of phosphate from water. *Chem. Eng. J.* **2015**, *268*, 270−279.

(15) Gu, W.; Xie, Q.; Xing, M.; Wu, D. Enhanced adsorption of phosphate onto zinc ferrite by incorporating cerium. *Chem. Eng. Res. Des.* **2017**, *117*, 706−714.

(16) Deng, H.; Yu, X. Adsorption of fluoride, arsenate and phosphate in aqueous solution by cerium impregnated fibrous protein. *Chem. Eng. J.* **2012**, *184*, 205−212.

(17) Hu, P.; Liu, Q.; Wang, J.; Huang, R. Phosphate removal by Ce(III)-impregnated crosslinked chitosan complex from aqueous solutions. *Polym. Eng. Sci.* **2017**, *57*, 44.

(18) Liu, X.; et al. Cerium oxide nanoparticle functionalized lignin as a nano-biosorbent for efficient phosphate removal. *RSC Adv.* **2020**, *10*, 1249−1260.
(19) Krajina, B. A.; Proctor, A. C.; Schoen, A. P.; Spakowitz, A. J.; Heilshorn, S. C. Biotemplated synthesis of inorganic materials: An emerging paradigm for nanomaterial synthesis inspired by nature. *Prog. Mater. Sci.* **2018**, *91*, 1−23.
(20) Nitz, M.; et al. Structural origin of the high affinity of a chemically evolved lanthanide-binding peptide. *Angew. Chem., Int. Ed.* **2004**, *43*, 3682−3685.
(21) Bentrop, D.; et al. Solution structure of the paramagnetic complex of the N-terminal domain of calmodulin with two Ce3+ ions by 1H NMR. *Biochemistry* **1997**, *36*, 11605−11618.
(22) Xu, M.; Su, Z.; Renner, J. N. Characterization of cerium (III) ion binding to surface-immobilized EF-hand loop I of calmodulin. *Pept. Sci.* **2019**, *111*, 2−7.
(23) Dixon, M. C. Quartz crystal microbalance with dissipation monitoring: Enabling real-time characterization of biological materials and their interactions. *Journal of Biomolecular Techniques* **2008**, *19*, 151−158.
(24) O'Sullivan, C. K.; Guilbault, G. G. Commercial quartz crystal microbalances - Theory and applications. *Biosens. Bioelectron.* **1999**, *14*, 663−670.
(25) Ye, Y.; Lee, H. W.; Yang, W.; Shealy, S.; Yang, J. J. Probing site-specific calmodulin calcium and lanthanide affinity by grafting. *J. Am. Chem. Soc.* **2005**, *127*, 3743−3750.
(26) Reviakine, I.; Johannsmann, D.; Richter, R. P. Hearing what you cannot see and visualizing what you hear: Interpreting quartz crystal microbalance data from solvated interfaces. *Anal. Chem.* **2011**, *83*, 8838−8848.
(27) Su, Z.; Pramounmat, N.; Watson, S. T.; Renner, J. N. Engineered interaction between short elastin-like peptides and perfluorinated sulfonic-acid. *Soft Matter* **2018**, *14*, 3528−3535.
(28) Quevedo, I. R.; Olsson, A. L. J.; Clark, R. J.; Veinot, J. G. C.; Tufenkji, N. Interpreting Deposition Behavior of Polydisperse Surface-Modified Nanoparticles Using QCM-D and Sand-Packed Columns. *Environ. Eng. Sci.* **2014**, *31*, 326−337.
(29) Quevedo, I. R.; Olsson, A. L. J.; Tufenkji, N. Deposition kinetics of quantum dots and polystyrene latex nanoparticles onto alumina: Role of water chemistry and particle coating. *Environ. Sci. Technol.* **2013**, *47*, 2212−2220.
(30) Suzin, L.; Antes, F. G.; Bedendo, G. C.; Bortoli, M.; Kunz, A. Chemical Removal of Phosphorus from Swine Effluent: the Impact of Previous Effluent Treatment Technologies on Process Efficiency. *Water, Air, Soil Pollut.* **2018**, *229*, 341.
(31) Huang, H.; et al. Simultaneous removal of ammonia nitrogen and recovery of phosphate from swine wastewater by struvite electrochemical precipitation and recycling technology. *J. Cleaner Prod.* **2016**, *127*, 302−310.
(32) Huang, H.; Yang, J.; Li, D. Recovery and removal of ammonia-nitrogen and phosphate from swine wastewater by internal recycling of struvite chlorination product. *Bioresour. Technol.* **2014**, *172*, 253−259.
(33) Liu, Y. H.; Kwag, J. H.; Kim, J. H.; Ra, C. S. Recovery of nitrogen and phosphorus by struvite crystallization from swine wastewater. *Desalination* **2011**, *277*, 364−369.
(34) Huang, W.; et al. Enhanced adsorption of phosphate by flower-like mesoporous silica spheres loaded with lanthanum. *Microporous Mesoporous Mater.* **2015**, *217*, 225−232.
(35) Tamura, H.; Mita, K.; Tanaka, A.; Ito, M. Mechanism of hydroxylation of metal oxide surfaces. *J. Colloid Interface Sci.* **2001**, *243*, 202−207.
(36) Wu, B.; Lo, I. M. C. Surface Functional Group Engineering of CeO2 Particles for Enhanced Phosphate Adsorption. *Environ. Sci. Technol.* **2020**, *54*, 4601.
(37) Tran, D. N. H.; Kabiri, S.; Wang, L.; Losic, D. Engineered graphene-nanoparticle aerogel composites for efficient removal of phosphate from water. *J. Mater. Chem. A* **2015**, *3*, 6844−6852.
(38) Xu, R.; Zhang, M.; Mortimer, R. J. G.; Pan, G. Enhanced Phosphorus Locking by Novel Lanthanum/Aluminum-Hydroxide Composite: Implications for Eutrophication Control. *Environ. Sci. Technol.* **2017**, *51*, 3418−3425.
(39) Hao, H.; Wang, Y.; Shi, B. NaLa(CO3)2 hybridized with Fe3O4 for efficient phosphate removal: Synthesis and adsorption mechanistic study. *Water Res.* **2019**, *155*, 1−11.
(40) Li, M.; Liu, J.; Xu, Y.; Qian, G. Phosphate adsorption on metal oxides and metal hydroxides: A comparative review. *Environ. Rev.* **2016**, *24*, 319−332.
(41) Zelmanov, G.; Semiat, R. The influence of competitive inorganic ions on phosphate removal from water by adsorption on iron (Fe+3) oxide/hydroxide nanoparticles-based agglomerates. *J. Water Process Eng.* **2015**, *5*, 143−152.
(42) Zheng, X.; et al. Fabrication of free-standing bio-template mesoporous hybrid film for high and selective phosphate removal. *Chem. Eng. J.* **2016**, *284*, 879−887.
(43) Zhang, Y.; Pan, B.; Shan, C.; Gao, X. Enhanced Phosphate Removal by Nanosized Hydrated La(III) Oxide Confined in Cross-linked Polystyrene Networks. *Environ. Sci. Technol.* **2016**, *50*, 1447−1454.
(44) Lin, J.; et al. Effect of calcium ion on phosphate adsorption onto hydrous zirconium oxide. *Chem. Eng. J.* **2017**, *309*, 118−129.
(45) Zhang, Y.; She, X.; Gao, X.; Shan, C.; Pan, B. Unexpected Favorable Role of Ca 2+ in Phosphate Removal by Using Nanosized Ferric Oxides Confined in Porous Polystyrene Beads. *Environ. Sci. Technol.* **2019**, *53*, 365−372.
(46) Wan, D.; et al. Adsorption of nitrate and nitrite from aqueous solution onto calcined (Mg-Al) hydrotalcite of different Mg/Al ratio. *Chem. Eng. J.* **2012**, *195-196*, 241−247.
(47) Wu, B.; Fang, L.; Fortner, J. D.; Guan, X.; Lo, I. M. C. Highly efficient and selective phosphate removal from wastewater by magnetically recoverable La(OH)3/Fe3O4 nanocomposites. *Water Res.* **2017**, *126*, 179−188.
(48) Li, T.; et al. Magnetic polymer-supported adsorbent with two functional adsorption sites for phosphate removal. *Environ. Sci. Pollut. Res.* **2019**, *26*, 33269−33280.
(49) Barth, A. Infrared spectroscopy of proteins. *Biochim. Biophys. Acta, Bioenerg.* **2007**, *1767*, 1073−1101.
(50) Rashidi Nodeh, H.; Sereshti, H.; Zamiri Afsharian, E.; Nouri, N. Enhanced removal of phosphate and nitrate ions from aqueous media using nanosized lanthanum hydrous doped on magnetic graphene nanocomposite. *J. Environ. Manage.* **2017**, *197*, 265−274.
(51) Liu, J.; Zhou, Q.; Chen, J.; Zhang, L.; Chang, N. Phosphate adsorption on hydroxyl-iron-lanthanum doped activated carbon fiber. *Chem. Eng. J.* **2013**, *215-216*, 859−867.

https://dx.doi.org/10.1021/acsestwater.0c00001
ACS EST Water 2021, 1, 58−67